The development pathway for $CD103^+CD8^+$ tissue-resident memory T cells of skin

Laura K. Mackay[1,5], Azad Rahimpour[1,5], Joel Z. Ma[1,5], Nicholas Collins[1], Angus T. Stock[1], Ming-Li Hafon[1], Javier Vega-Ramos[1], Pilar Lauzurica[2], Scott N. Mueller[1], Tijana Stefanovic[3], David C. Tscharke[3], William R. Heath[1], Michael Inouye[1,4], Francis R. Carbone[1,6] & Thomas Gebhardt[1,6]

[1]Department of Microbiology and Immunology, The University of Melbourne, Parkville, Victoria 3010, Australia

[2]Instituto de Salud Carlos III, Majadahonda, Madrid 28220, Spain

[3]Division of Biomedical Science and Biochemistry, Research School of Biology, The Australian National University, Canberra, ACT 0200, Australia

[4]Department of Pathology, The University of Melbourne, Melbourne Victoria 3010, Australia

[5]These authors contributed equally to this work

[6]These authors are co-senior authors

Correspondence should be addressed to F.R.C. (fcarbone@unimelb.edu.au) or T.G. gebhardt@unimelb.edu.au.

Tissue-resident memory T cells (T_{RM}) provide superior protection against infection in extra-lymphoid tissues. Here we show that $CD103^+CD8^+$ T_{RM} cells developed in the skin from killer cell lectin-like receptor G1 (KLRG1)-negative precursors that selectively infiltrate the epithelial layer. A combination of epithelial entry in addition to interleukin 15 (IL-15) and transforming growth factor-β (TGF-β) signaling was required for formation of these long-lived memory cells. Importantly, T_{RM} differentiation resulted in the progressive acquisition of a unique transcriptional profile that differed from those expressed by circulating memory cells and other types of T cells that permanently reside in skin epithelium. We provide a comprehensive molecular framework for the local differentiation of a distinct peripheral memory population that forms a first-line immune defense system in barrier tissues.

Introduction

Infection primes a population of effector T cells that migrate to all manner of peripheral tissues. The entry of these cells is controlled via a migration-imprinting program dependent on the origin of infection and by the induction of local chemokines that recruit T cells into sites of active inflammation[1]. As the infection resolves and local inflammation subsides, T cell infiltration into non-lymphoid organs gradually declines[2,3] partly as a consequence of transient expression of the homing receptors that permit trafficking into organs such as gut and skin[4-6]. Nonetheless, long-term T cell immunity can be maintained in regional tissues due to the action of a subset of cells that lodge during the early phase of peripheral infection and thereafter never return to the circulation[7,8]. These are termed tissue-resident memory T cells (T_{RM}), with the best characterized being $CD8^+$ memory T cells bearing the α-chain (CD103) of the $\alpha_E\beta_7$ integrin[9]. Such $CD103^+CD8^+$ T_{RM} cells have been identified in different tissues[9-11] where they can dominate immunity against a variety of localized infections[5,9,12-15].

Memory T cells in the blood and secondary lymphoid organs have been defined as belonging to the lymphoid tissue-recirculating central memory (T_{CM}) and extra-lymphoid tissue-infiltrating effector memory (T_{EM}) subsets[16]. While some peripheral T cells are

likely to equilibrate with the blood, some do not[17], and the latter belong to the T_{RM} category[4, 9, 13]. At the current time, it remains unclear how the T_{EM}, T_{CM} and T_{RM} subsets are related. There exists considerable information about the developmental processes that give rise to the distinct T_{EM} and T_{CM} populations[18,19], although how T_{RM} cells fit into these lineages remains unclear. It is known that T_{RM} cells lodge during the effector phase of the immune response[4,9], at a time when memory precursors are present in the circulation. Such precursors can be defined by their differential expression of the molecules, killer cell lectin-like receptor family G member 1 (KLRG1) and interleukin-7 receptor α-chain (CD127). Long-lived circulating memory cells are progressively derived from $KLRG1^{-}CD127^{lo}$ and $KLRG1^{-}CD127^{hi}$ precursors, while $KLRG1^{+}CD127^{-}$ cells give rise to short-lived effector or effector-like memory populations[18-20]. Since tissue T cells are known to have enhanced effector capabilities[21], one might have predicted that T_{RM} would originate from the $KLRG1^{+}$ precursors. However unlike circulating effectors, $CD103^{+}CD8^{+}$ T_{RM} are particularly long-lived, meaning that their origins are more likely to be the $KLRG1^{-}$ precursors that give rise to persisting memory cells, such as the T_{CM} found in the circulation.

In order to clearly define T_{RM} development, it is necessary to understand what controls precursor entry into non-lymphoid compartments. $CD103^{+}CD8^{+}$ T_{RM} cells often reside in the epithelium in a range of different tissues including the gut, skin and female reproductive tract[9,22,23]. This specific localization of T_{RM} cells may be linked to the production of transforming growth factor (TGF)-β in these environments[24,25] as this cytokine is a major driver of CD103 expression[26-28]. As a consequence, one would predict that migration into epithelium would be a critical step in $CD103^{+}CD8^{+}$ T_{RM} cell maturation. Here, we show that this prediction holds true for the skin, with entry into the epidermis being a pivotal transition point for successful T_{RM} maturation. We exploit this requirement for epidermal entry to characterize the development of T_{RM} cells, and to differentiate these memory cells from their T_{CM} and T_{EM} counterparts in lymphoid tissues.

Results

The roles of CD69 and CD103 in T_{RM} development

To analyze the formation of $CD103^+CD8^+$ T_{RM} cells in skin, we used infection with herpes simplex virus (HSV) in combination with adoptive transfer of T cell receptor (TCR) transgenic gBT-I cells specific for this pathogen. Tracking gBT-I cells by their expression of V$_{\alpha}$2, CD45.1 and/or CD45.2 revealed their rapid accumulation in infected skin, with numbers peaking around day 7 and then rapidly falling thereafter (**Fig. 1a**). In contrast, $CD103^+$ gBT-I numbers increased at a more modest rate to reach a stable plateau around 2 weeks after infection. Consistent with their lack of contraction, $CD103^+$ T_{RM} cells up-regulated the pro-survival molecule, Bcl-2 (**Fig. 1b**). Skin-infiltrating gBT-I cells also up-regulated CD69 (**Fig. 1c**), which preceded the expression of CD103 (**Fig. 1d**). Analogous patterns of progressive Bcl-2, CD69 and CD103 up-regulation were also found in endogenous non-transgenic T cells (**Supplementary Fig. 1a**,**b**). Separating the skin into epidermis and dermis at day 11 after infection showed that virus-specific T cells had heterogeneous CD69 expression in the dermis but were nearly all $CD69^+$ in the epidermis (**Fig. 1e**). At the same time, a large portion of epidermal gBT-I cells expressed CD103 while their counterparts in the dermis were predominantly $CD103^-$ (**Fig. 1e**). It should be noted that dermis preparations contain hair follicles with residual epithelial cells, including intra-epithelial T cells (**Supplementary Fig. 1c**).

Both CD69 and CD103 were necessary for optimal formation and/or survival of $CD8^+$ T_{RM} cells in the skin, since deletion of these molecules resulted in reduction in T_{RM} numbers after adoptive co-transfers of equal numbers of wild-type and CD69 (*Cd69*$^{-/-}$) or CD103 (*Itgae*$^{-/-}$) knock-out gBT-I cells prior to infection (**Fig. 1f**,**g**). CD69 was also necessary for T cell persistence in the sensory ganglia (**Supplementary Fig. 1d**). Given the sequential nature of CD69 and CD103 induction (**Fig. 1d**), we contended that the absence of the individual molecules would affect T_{RM} development in a progressive fashion, with loss of CD69 having an early impact while CD103 deletion would have a downstream effect on T cell numbers. Indeed, *Cd69*$^{-/-}$ gBT-I cells were lost at a much faster rate than *Itgae*$^{-/-}$ gBT-I cells (**Fig. 1g**). In both cases, starting ratios of wild-type-to-knock out cells in skin and spleen were roughly 1, with the latter remaining close to 1 at

all times examined. Histology showed that CD103 was dispensable for T cell entry into the epidermis, since both wild-type and *Itgae*$^{-/-}$ gBT-I cells could reach this compartment (**Supplementary Fig. 1e**). The combined results suggested that CD69 deficiency had an impact shortly after T cells entered the skin, while CD103 deletion affected T_{RM} cell persistence long after the cells had reached the epidermis.

T_{RM} cells derive from KLRG1^{-} precursor cells

After skin infection with HSV, there was a gradual shift of gBT-I cells in the spleen from CD62L^{-}CD127^{-}KLRG1^{+} effectors to a predominantly CD62L^{+}CD127^{+}KLRG1^{-} T_{CM} population at late times (1 year) after infection, with heterogeneous populations of T_{CM} and T_{EM} cells (CD62L^{-}CD127$^{+/-}$KLRG1^{+}) at intermediate times (**Supplementary Fig. 2a**). Changes were also seen in skin T cells when we examined expression of KLRG1 and CD103 (**Fig. 2a**). Early after infection (week 1), skin T cells were predominantly KLRG1^{+}CD103^{-} effectors, while at memory times (week 4) the surviving memory cells were almost exclusively CD103^{+} T_{RM} cells with little or no KLRG1 expression (**Fig. 2a**), as described for T_{RM} cells in other organs[11,22]. Endogenous CD103^{+} T cells in the skin also largely lacked expression of KLRG1 (**Supplementary Fig. 2b**). While greater than 50% of splenic gBT-I cells were KLRG1^{+} 4 weeks after infection, less than 7% of the corresponding skin T cells expressed this marker (**Fig. 2a**). This difference was consistent with previous studies showing disequilibrium between T_{RM} cells in the skin and the circulating memory cells and, in particular, cells of a T_{EM} phenotype (which largely express KLRG1) that survive through to memory times[5,13].

These data supported the hypothesis that the skin CD103^{+} T_{RM} population developed from KLRG1^{-} precursors. Consistent with this, separation of skin into dermis and epidermis at early times after infection showed that the latter consisted almost exclusively of KLRG1^{-} gBT-I cells, whereas the former contained a mixture of KLRG1^{-} and KLRG1^{+} cells, similar to what was found in the spleen (**Fig. 2b**,**c**). To better visualize the localization of the different populations, acutely infected skin was examined by immunofluorescence microscopy for KLRG1 expression (**Fig. 2d**). In these sections, the KLRG1^{+} gBT-I cells exhibited a weaker but clearly discernable fluorescence signal (**Fig.**

2d, yellow arrows), in contrast to an undefined population with strong fluorescence. Confirming the flow cytometric analysis, virtually all gBT-I cells in the epidermis and the majority in the upper regions of the dermis lacked expression of KLRG1 (**Fig. 2d**, red arrows). Finally, adoptive transfer of gBT-I effector cells isolated from spleen 6 days after infection and sorted into $KLRG1^+$ and $KLRG1^-$ subsets, showed that only the latter could generate $CD103^+$ T_{RM} cells in the skin of infected recipients (**Fig. 2e**). These data formally demonstrated that $KLRG1^-$ precursor cells could give rise to intra-epithelial T_{RM} cells in skin. $KLRG1^-$ cells also preferentially generated T_{RM} cells in the sensory ganglia (**Supplementary Fig. 2c**), thus implicating them as broad T_{RM} precursors.

T_{RM} formation requires epithelial infiltration

Our data implied that epithelial infiltration and T_{RM} formation by virus-specific $CD8^+$ T cells were functionally linked; however, it fell short of demonstrating that epithelial entry was indeed required for T_{RM} maturation. In order to examine the migration of T cells from the dermis to the epithelium independent of their initial priming or recruitment from the blood, we directly injected *in vitro* activated gBT-I cells into the dermis to test if these cells could develop into epithelial-lodged $CD103^+$ T_{RM} cells. The population of injected cells gradually increased expression of CD69 and CD103 (**Supplementary Fig. 3a**) and concomitant with these phenotypic changes, eventually localized to the epidermis and hair follicle epithelium (**Supplementary Fig. 3b**). To show that epidermal entry was necessary for T_{RM} formation, we treated the *in vitro* activated T cells with pertussis toxin (PTx) prior to intradermal injection into flank skin. PTx inactivates G protein-coupled receptors, thereby blocking chemokine-driven migration[29]. While untreated cells gave rise to a population of $CD69^+CD103^+$ T_{RM} cells after intradermal injection, PTx treatment blocked both epithelial infiltration and *in vivo* CD103 expression (**Fig. 3a**,**b** and **Supplementary Fig. 3c**). PTx-treated gBT-I cells were still able to up-regulate CD103 when exposed to TGF-β *in vitro* (**Supplementary Fig. 3d**), arguing that the lack of up-regulation *in vivo* resulted from a migration defect rather than an intrinsic block in CD103 expression *per se*. Combined, these data argue that migration to the epithelium is necessary for skin $CD103^+CD8^+$ T_{RM} development.

Chemokines regulate epidermal entry of T_{RM} precursors

We next sought to identify chemokines that promote entry into the epidermis and thus T_{RM} formation. CXCL9 and CXCL10 have previously been shown to facilitate entry into the epithelium during HSV-2 infection of mucosal surfaces[15] and mRNAs encoding these chemokines were synthesized by keratinocytes during HSV skin infection (**Supplementary Fig. 4a**). Importantly, the KLRG1$^-$ T_{RM} precursors showed preferential migration towards these chemokines in transwell assays *ex vivo* (**Fig. 3c** and **Supplementary Fig. 4b**), which was consistent with higher expression of the CXCL9/10 receptor CXCR3 on this subset as compared to KLRG1$^+$ effector cells (**Fig. 3d**). Intradermal injection of *in vitro* activated CD8$^+$ T cells lacking CXCR3 expression (*Cxcr3*$^{-/-}$) resulted in the generation of fewer CD103$^+$ T_{RM} cells compared to injection of wild-type populations (**Fig. 3e**, left). This decrease was not a consequence of poor survival of the *Cxcr3*$^{-/-}$ T cells, since they were found in higher frequency in lymphoid organs (**Fig. 3e**, left), suggesting a more efficient return to the circulation. Given the latter, we sought to determine what happens when we blocked egress from the skin. It is known that CCR7 is required for tissue exit via the lymphatics[30,31], so we reasoned that CCR7-deficient cells might give rise to greater numbers of CD103$^+$ T_{RM} cells. Indeed, *Ccr7*$^{-/-}$ CD8$^+$ T cells displayed increased T_{RM} formation as compared to their wild-type counterparts, with a concomitant decrease in their return to the lymph nodes (**Fig. 3e**, right). Thus, it appears that facilitating entry of T cells into the epidermis or inhibiting their egress from the skin promotes CD103$^+$ T_{RM} formation.

TGF-β and IL-15 are required for T_{RM} development in skin

TGF-β, which is expressed in the skin epithelium[24], is a known driver of CD103 up-regulation and has been shown to be important in promoting T_{RM} maturation in other tissues[28]. However, its contribution to T_{RM} formation in the skin is unknown. Thus, we wanted to examine what effect TGF-β receptor (TGF-R) signaling had on skin T_{RM} formation. Initial experiments involved direct intradermal injection of wild-type and TGF-R type II-deficient (*Tgfbr2f/f*.dLck-Cre) OT-I cells that were activated by splenocytes coated with the cognate ovalbumin peptide prior to transfer. After intradermal injection, only the wild-type OT-I cells up-regulated CD103 (**Fig 4a**, top). In

addition to the lack of CD103 expression, the TGF-R-deficient cells were also selectively lost from the skin but not the spleen (**Supplementary Fig. 5a**). We verified that TGF-R was also required for CD103 up-regulation after infection. Here, a mixture of wild-type and *Tgfbr2f/f*.dLck-Cre OT-I cells were transferred into C57BL/6 mice and then infected with recombinant HSV expressing ovalbumin. CD103 up-regulation was only seen on skin-infiltrating wild-type cells, whereas *Tgfbr2f/f*.dLck-Cre cells lacked expression of this integrin subunit and gradually disappeared from the skin (**Fig. 4a**, bottom, and **4b**).

$CD103^+$ T_{RM} cell formation and/or survival was also IL-15-dependent, since its absence resulted in decreased T_{RM} numbers compared to wild-type controls (**Fig. 4c**). In these experiments, effector gBT-I cells were primed in wild-type donors and re-transferred into infected wild-type or IL-15-deficient ($Il15^{-/-}$) recipients in order to minimize a potential impact of initial T cell priming in the absence of IL-15. Reduced T_{RM} formation in $Il15^{-/-}$ mice was evident by 2 weeks after infection, with very low numbers of T_{RM} cells present in skin of $Il15^{-/-}$ mice by week 4, and similarly also in the dorsal root ganglia (**Supplementary Fig. 5b**). This reduction correlated with a muted induction of Bcl-2 in $CD103^+$ skin T cells in the absence of IL-15 (**Supplementary Fig. 5c**). IL-15-dependence was also seen with splenic memory cells, although to a lesser extent than with the skin T_{RM} cells (**Fig. 4c**). T_{RM} generation was completely restored in bone marrow chimeric mice in which IL-15 production was restricted to radio-resistant cells (**Fig. 4d**). Thus, IL-15 from radio-resistant cells such as skin keratinocytes and Langerhans cells is sufficient to support optimal T_{RM} development and survival.

A unique transcriptional profile of T_{RM} cells

While transcriptional analysis of T_{EM} and T_{CM} cells have been published[32], there exists no comparison between these transcriptomes and that for the T_{RM} subset. Given this, we carried out microarray expression analysis of $CD103^+CD8^+$ T_{RM} cells from skin, gut and lung using respective infections with HSV, lymphocytic choriomeningitis virus (LCMV) and influenza virus comparing them to T_{CM} and T_{EM} cells isolated from HSV-infected animals. To facilitate memory subset identification and isolation, we used TCR-transgenic T cells of desired specificity, transferring them to C57BL/6 mice prior to

infection. For HSV and LCMV infections we used mice adoptively transferred with T cells specific for natural virus determinants (from gBT-I and P14 mice, respectively), while for influenza virus infection we used a recombinant virus (flu.gB) expressing the HSV glycoprotein B (gB) in combination with gBT-I cells. Since our study had focused on skin T_{RM} cells, we also included two other skin-resident intra-epithelial T cell subsets in these comparisons: γδ-TCR-expressing dendritic epidermal T cells (DETCs) and a population of αβ-TCR-bearing cells that populate the epidermal niche in mice that lack γδ-DETCs (*Tcrd*$^{-/-}$ mice).

The transcriptional data was subjected to principle-component analysis (PCA) (**Fig. 5a**) to delineate variations in the data and the similarities/distances between T cell subsets were calculated using a mutual information (MI) approach (**Fig. 5b**). The PC1 and PC2 axes of variation in the PCA clearly differentiated the circulating T cell subsets from those that are resident or DETC-like (**Fig. 5a**). This pattern was consistent with the pairwise relationships defined by the MI analysis (**Fig. 5b**), which showed that T_{RM} cells from different tissues were transcriptionally related. The PCA showed that the transcriptomes of the T_{EM} and T_{CM} subsets were most similar to that of naïve T cells rather than T_{RM} cells, which were themselves distinct from the γδ- and αβ-DETCs. Thus, both the PCA- and MI-based metrics demonstrated that the various T_{RM} populations formed a transcriptomically distinct subset that as a group were less similar to the T_{EM} and T_{CM} subsets than the T_{EM} and T_{CM} subsets were to each other or to circulating naïve T cells.

A detailed comparison of genes differentially regulated in the T_{RM} versus circulating memory subsets is shown in **Figure 5c**,**d**. For this comparison, we used combined thresholds of 1.5 log-fold change in gene expression and *P*-values of <0.05 to identify genes that were differentially expressed between the circulating and resident memory populations. Each T_{RM} subset had unique elements, with between 25 to 127 transcripts specific for each of the individual T_{RM} populations from the different tissues (**Fig. 5c**) such as those for CCR9 (expressed only in gut T_{RM} cells) and CCR8 (expressed only in skin T_{RM} cells). Common transcript expression was also found in T_{RM} populations,

between 51 and 73 transcripts shared between any given pair. These included transcripts, such as that for the aryl hydrocarbon receptor (*Ahr*), which were selectively up-regulated in gut and skin T_{RM} cells but not the corresponding population in the lung. Importantly, the comparison identified 37 transcripts commonly up- or down-regulated between all three T_{RM} subsets (**Fig. 5c,d** and **Table 1**). 60% of the differentially expressed transcripts were up-regulated on T_{RM} cells compared to circulating memory T cells, although some key molecules were down-regulated, including the sphingosine 1-phosphate receptor 1 ($S1PR_1$). Overall, these 37 transcripts and their products differentiated T_{RM} cells from their counterparts in the circulation and thus, represented the core transcriptional signature for this population.

Progressive engagement of the T_{RM} transcriptome

Finally we tracked the changes in the expression of selective genes as T cells progressed along the T_{RM} maturation pathway in the skin. From the results above, we predicted that T_{RM} cells mature from the time they enter the dermis at the peak of the effector response, through to their recruitment into the epidermis and finally, their acquisition of surface expression of CD103 (schematic in **Supplementary Fig. 6)**. We focused on $KLRG1^-$ T cells in this analysis since neither skin T_{RM} cells, nor their precursors, expressed KLRG1. T cells were isolated from the dermis and/or epidermis at either the height of the effector response (day 8) after HSV infection, or at the start of memory conversion (day 14). Quantitative PCR analysis of genes commonly regulated in all (*Cdh1, S1pr1, Tlr1, Itga1, Itgae, Cd244*) or selected (*Ccr8* and *Ahr*) T_{RM} subsets showed appropriate up- or down-regulation as the cells progressed along this putative maturation pathway in skin (**Fig. 5e**). Overall, this analysis tracked the transcriptional development of T_{RM} cells from early $KLRG1^-$ effector-type precursors to fully mature $CD103^+$ T_{RM} cells lodged in the epidermis.

Discussion

This study provides one of the first detailed descriptions of $CD103^+CD8^+$ T_{RM} development and extended phenotype. It defines a maturation pathway for skin T_{RM} cells from $KLRG1^-$ precursors that enter the tissues during the early effector response, with an

important checkpoint being their migration into the epidermis in a chemokine-dependent manner. IL-15 and TGF-β are involved in skin T_{RM} formation and/or survival, with the latter likely driving CD103 up-regulation, consistent with what has been found in a variety of other tissues[27,28,33]. The T_{RM} precursors are not end-stage differentiated effectors or mature T_{EM} cells. Both these latter populations express KLRG1[19,20], whereas the $CD8^+$ T_{RM} precursors reaching the epithelium and the mature skin-resident memory cells do not. Once formed, the T_{RM} cells do not appear to undergo any contraction, but instead remain numerically stable over a considerable time[5,14,21]. With respect to this longevity, $CD103^+CD8^+$ T_{RM} cells appear more closely related to the circulating T_{CM} cells, rather than the shorter-lived T_{EM} cells that are ultimately lost from the circulation[34,35]. This matches their derivation from $KLRG1^-$ precursors, which are also the origin of the long-lived T_{CM} population[20,36,37]. In addition, T_{RM} cells appear capable of proliferating *in situ* on re-stimulation[38,39] and, although not universal[11], in some cases after *in vivo* transfer[22]; attributes typically associated with the T_{CM} subset[35].

Entry into the epidermis involved the action of CXCR3 ligands, although additional molecules are likely to also participate in this event since the absence of CXCR3 did not completely abrogate T_{RM} formation. Nonetheless, the proposal for CXCR3-mediated epithelial recruitment is consistent with the recent finding that exogenous application of CXCR3 ligands can promote T_{RM} formation in the epithelium of the lower female reproductive tract[15]. T_{RM} formation was enhanced in the absence of CCR7 expression on T cells introduced directly into skin, probably as a consequence of reduced precursor return to the circulation since CCR7 promotes T cell egress from the skin and other tissues[30,40]. Such a scenario suggests that the precursors are not fully committed to the T_{RM} fate when they first enter the skin.

While transcriptional analysis of brain T_{RM} cells has been described previously[41], the broader comparison used here uniquely identified just under 40 transcripts that define a core differential gene-set for this population. One of the differential transcripts is the $S1PR_1$ gene product, which controls T cell entry into lymphatics[42] and requires down-regulation in order to retain T_{RM} cells in peripheral tissues[43]. Complementing this, CD69

is rapidly up-regulated once the T cells reach the skin, which provides additional impetus for tissue retention since this molecule is known to functionally inhibit $S1PR_1$[44]. We showed that CD69 independently affects T_{RM} numbers, similar to what has been shown for $CD103^+CD8^+$ T cells in the lung[27]. However, while previously it was thought that loss of CD69 inhibited ongoing T cell recruitment[27], the data here suggest that it affects early T_{RM} precursor retention. The microarray analysis also showed that a second member of the S1P receptor family, $S1PR_5$, was down-regulated. In contrast to $S1PR_1$, $S1PR_5$ is not inhibited by CD69[45]. Additional gene products associated with tissue retention are RGS-1 and RGS-2, both known G protein-coupled inhibitors[46]. Separately, T_{RM} up-regulate the molecules CD49a, E-cadherin and $\alpha_E\beta_7$, all associated with cell tethering or adhesion[47]. Overall, the results show that down-regulation of tissue egress appears to be a critical feature of $CD103^+CD8^+$ T_{RM} maturation.

While tissue retention is a central feature of the T_{RM} phenotype, the array data argues that these are not simply circulating memory cells trapped within the extra-lymphoid environs. Instead T_{RM} cells are a phenotypically distinct population. For example, genes associated with the modulation of T cell signaling are also present in the core transcriptional gene-set and absent from the circulating memory subsets. The immune modifiers CTLA-4, ICOS, KLRE1 and various members of the SLAM family of molecules along with transcription factors such as Nr4a members and Litaf, are all differentially regulated in T_{RM} cells. Combined, this points to a distinct phenotype for the resident subset. This was reinforced by the PCA and pair-wise MI analyses, which showed that the T_{RM} transcriptomes differed from those of the circulating memory subsets. Interestingly, the bioinformatics analysis also showed that the skin T_{RM} cells differed from the main intra-epithelial T cells naturally found in mouse skin, notably the γδ-DETCs and the αβ-TCR-expressing cells that fill the void in the absence of the former. To some extent, this makes sense since both sets of DETCs are involved in innate processes such as skin homeostasis and wound-healing[48,49] rather than contributing to adaptive immunity and immune memory as do the $CD103^+CD8^+$ T_{RM} cells[8].

Overall, the gene expression and maturational tracking studies show that T_{RM} cells are derived from the same precursors that give rise to the long-lived memory cells found in the circulation. The memory precursors undergo an *in situ* developmental program that results in their differentiation to specialized memory cells adapted to the extra-lymphoid compartment. T_{RM} development is not a default program, but instead is location dependent, requiring the action of tissue-specific cytokines and, in some cases, local antigen recognition[11,14]. As a consequence, T_{RM} cells are focused on regional immunity, consistent with the emerging view that they provide superior peripheral infection control[9,13,14]. By identifying the T_{RM} precursors and describing mechanisms associated with their retention and maturation, we provide the foundation for studies designed to manipulate T_{RM} generation and lodgment for the purpose of enhanced immune protection.

Author contributions

L.K.M., F.R.C. and T.G. designed the experiments; L.K.M., A.R., J.Z.M., N.C., A.T.S., M.H. and T.G. did the experiments; L.K.M., A.R., J.Z.M., A.T.S., W.R.H., M.I. F.R.C. and T.G. analyzed the data; J.V., P.L., S.N.M., T.S. and D.C.T. contributed reagents. F.R.C. led the research program and wrote the manuscript with the help of L.K.M. and T.G.

Acknowledgements

We thank W. Weninger (University of Sydney, Australia) for *Ccr7*$^{-/-}$ mice; N. Hunt (University of Sydney, Australia) for *Cxcr3*$^{-/-}$ mice and M. Bevan (University of Washington, USA) for OT-I.*Tgfbr2f/f*.dLck-Cre mice. We also thank members of the Carbone and Heath laboratories for discussions and N. McBain and J. Smith (University of Melbourne, Australia) for excellent technical assistance. Supported by National Health and Medical Research Council of Australia and Australian Research Council.

Accession codes

GEO accession number is GSE47045.

Competing financial interests

The authors declare no financial competing interests.

Figure Legends

Figure 1. CD103 and CD69 regulate T_{RM} lodgement and persistence. (**a**–**e**) Mice that received naïve gBT-I cells were subjected to HSV infection. gBT-I cells were tracked throughout the response based on their expression of V$_\alpha$2, CD45.2 and CD45.1. (**a**) Enumeration of total and CD103$^+$ gBT-I cells in skin at different times p.i; data pooled from 3 experiments (*n* = 8–12 mice/group). (**b**) CD103 and Bcl-2 expression by gBT-I cells at the indicated times p.i.; data representative of 3 experiments. Plots are gated on gBT-I cells; numbers depict percentage of events in respective gates (as in **c**,**e**). (**c**,**d**) Analysis of CD103 and CD69 expression by gBT-I cells in skin at the indicated times p.i.; data representative of *n* = 4–12 mice/time point. (**e**) CD103 and CD69 expression by gBT-I cells in the epidermis (Epi) and dermis (Derm) 11 d p.i. Histograms representative of *n* = 4 mice. (**f**) Wild-type (WT) and *Cd69*$^{-/-}$ or *Itgae*$^{-/-}$ gBT-I cells expressing distinct patterns of CD45.1 and CD45.2 were co-transferred or transferred into separate mice prior to HSV infection. Representative plots show gBT-I cells in spleen (gated on CD8$^+$ cells) and skin (gated on V$_\alpha$2$^+$ cells) >30 d p.i. (**g**) Ratios of WT to *Cd69*$^{-/-}$ or *Itgae*$^{-/-}$ cells at the indicated times p.i.; data pooled from 3 experiments (*n* = 9–12 mice/group).

Figure 2. T_{RM} cells develop from KLRG1$^-$ precursors that selectively infiltrate the epidermis during acute infection. (**a–d**) Mice received naïve gBT-I.CD45.1 or gBT-I.GFP cells prior to HSV infection. (**a**) CD103 and KLRG1 expression by gBT-I cells in skin and spleen during acute infection (1 wk), after infection resolution (2 wks) and during early memory (4 wks). Plots are gated on V$_\alpha$2$^+$CD45.2$^+$CD45.1$^+$ events and are representative of 3 experiments (*n* = 12 mice/time point). Numbers depict percentage of events in respective gates (as in **b**). (**b**,**c**) KLRG1 expression by gBT-I cells isolated from the epidermis (Epi), the dermis (Derm) and the spleen at various times p.i. (6.5 d p.i. in **b**). Data pooled from 2 experiments (*n* = 8–9 mice/time point). (**d**) Microscopy analysis of KLRG1 expression in acutely infected skin (d 6 p.i.) after staining with fluorescently labeled anti-KLRG1 antibodies. gBT-I cells are identified by GFP expression and depicted in the bottom panel; yellow and red arrows indicate examples of KLRG1$^+$ and KLRG1$^-$ gBT-I cells, respectively. Dashed lines indicate the epidermal-dermal junction. Photos are representative of 2 experiments. Scale bars, 100 μm. (**e**) Effector gBT-I cells

were sorted into KLRG1$^+$ and KLRG1$^-$ subsets from spleens of infected mice (6 d p.i.) and transferred into infected recipients (4 d p.i.). Enumeration of CD103$^+$ gBT-I cells in skin 3 wks p.i.; data pooled from 3 experiments (n = 12 mice/group); *, $P < 0.05$ by two-tailed Mann-Whitney test.

Figure 3. Opposing chemokines regulate epidermal entry and T_{RM} differentiation versus tissue egress. (**a**,**b**) *In vitro* activated gBT-I cells were left untreated (Ctrl) or PTx-treated, and transferred intradermally into separate mice. (**a**) CD103 and CD45.1 expression by CD45.2$^+$ cells isolated from the epidermis (Epi) and dermis (Derm) 8 d post-transfer. gBT-I cells were identified as V$_\alpha$2$^+$CD45.1$^+$ events (in upper quadrants). Numbers depict percentage of events in respective gates (as in d). (**b**) Enumeration of CD103$^+$ gBT-I cells from total skin preparations at the indicated times after transfer. Data pooled from 2 experiments (n = 6 mice/group). **, $P < 0.01$ by two-tailed Mann-Whitney test. (**c**) *Ex vivo* migration towards CXCL10 gradients by KLRG1$^+$ and KLRG1$^-$ effector gBT-I cells enriched from spleen 7 d p.i.; data pooled from 5 experiments with 5 donor mice/experiment. (**d**) CXCR3 expression by KLRG1$^+$ and KLRG1$^-$ effector gBT-I cells isolated from spleen (6.5 d p.i.). Histogram is representative of 2 experiments. (**e**) Analysis of CD8$^+$ T cells in draining lymph nodes (dLN) and skin (CD103$^+$ T_{RM}) at different times after *in vitro* activation and intradermal transfer. Depicted are the ratios of CD8$^+$ effector T cells generated from *Cxcr3*$^{-/-}$ or *Ccr7*$^{-/-}$ mice relative to that of co-transferred effector cells from WT mice. Data pooled from 2–3 experiments (n = 7–12 mice/group). **, $P < 0.01$; ***, $P < 0.001$; ****, $P < 0.0001$ by two-tailed paired t-test.

Figure 4. TGF-β receptor and IL-15 signaling is required for CD103$^+$ T_{RM} cell development. (**a**) CD103 expression by WT and *Tgfbr2f/f*.dLck-Cre OT-I cells in skin after *in vitro* activation and intradermal transfer (top) or naïve cell transfer and HSV.OVA infection (bottom), at the indicated times. Plots are gated on OT-I cells; numbers depict percentage of events in respective gate. (**b**) Ratios of WT to *Tgfbr2f/f*.dLck-Cre OT-I cells in skin and spleen at the indicated times p.i.; data pooled from 2 experiments (n = 10–11 mice per group). (**c**,**d**) Effector gBT-I cells were enriched from spleens of WT mice 6 d p.i. and transferred into infected (4 d p.i.) WT, *Il15*$^{-/-}$ or

various combinations of bone marrow chimeric mice, as indicated. (**c**) Enumeration of $CD103^+$ gBT-I cells in WT and *Il15*$^{-/-}$ mice at different times p.i. Data pooled from 3–4 experiments (n = 11–12 mice/group). **, $P < 0.01$; ***, $P < 0.001$; ****, $P < 0.0001$ by two-tailed Mann-Whitney test. (**d**) Enumeration of $CD103^+$ gBT-I cells in the skin of various bone marrow chimeric mice. Data pooled from 2 experiments analyzed 3 and 6 wks p.i. (n = 8–10 mice/group). *, $P < 0.05$; **, $P < 0.01$; ***, $P < 0.001$ by Kruskal-Wallis test followed by Dunns multiple comparison post test.

Figure 5. Definition of a core transcriptional profile of T_{RM} cells that is progressively engaged during differentiation. (**a**) PCA of gene expression data from various subtypes of lymphoid and peripheral $CD8^+$ T cells (as labeled in plot and key). Circles group the T cell types into 3 distinct clusters. (**b**) Mutual information analysis of the genome-wide gene expression distributions for a pair of cell types. (**c**) Gene expression of T_{RM} cells from skin, lung and gut was compared in a pair-wise fashion to that of T_{CM} and T_{EM} cells. Differentially expressed transcripts (≥ 1.5 log fold change and a Benjamini Hochberg-adjusted $P < 0.05$) shared by each T_{RM} type are indicated in the overlapping regions of the Venn diagram. (**d**) Heat map of gene expression for differentially expressed transcripts in the lymphoid (Circulation) compared to the group T_{RM} group (Periphery). (**e**) Mice received naïve gBT-I cells prior to HSV infection. gBT-I cells from the skin 8 d and 14 d p.i. were sorted into $KLRG1^-$ subsets as indicated (Sk, total skin; Der, dermis; Epi, epidermis). qPCR analysis of selected genes during T_{RM} differentiation. Median values were calculated relative to *Hprt* and normalized to T_{RM} values. Data pooled from 2–5 experiments.

Table 1. List of gene transcripts defining the T_{RM} core signature. List of 37 transcripts commonly regulated in T_{RM} cells from the skin, gut and lung, and differentially expressed compared to both T_{CM} and T_{EM} cells from the spleen. These transcripts represent the overlapping region of the Venn diagram in **Figure 5c** and the heat map in **Figure 5d**.

Methods

Mice

C57BL/6, B6.SJL-PtprcaPep3b/BoyJ (B6.CD45.1$^+$), gBT-I×B6.CD45.1 (gBT-I.CD45.1$^+$CD45.2$^+$), gBT-I.GFP, OT-I×B6.CD45.1 (OT-I.CD45.1$^+$CD45.2$^+$), P14×B6.CD45.1 (P14.CD45.1$^+$CD45.2$^+$), *Il15*$^{-/-}$mice, gBT-I.*Itgae*$^{-/-}$, gBT-I.*Cd69*$^{-/-}$ and *Tcrd*$^{-/-}$ mice were bred in the Department of Microbiology and Immunology in The University of Melbourne (Melbourne, Australia). Female mice between the age of 6-12 weeks were used for experiments. The gBT-I and OT-I mice are CD8$^+$ TCR transgenic mice that recognize the H-2K^b-restricted HSV-1 gB epitope of amino acids 498-505 ($gB_{498\text{-}505}$) and the ovalbumin-derived epitope of amino acids 257-264 ($OVA_{257\text{-}264}$), respectively. gBT-I.*Cd69*$^{-/-}$ were generated by back-crossing gBT-I mice with *Cd69*$^{-/-}$ animals obtained from P. Lauzurica (Instituto de Salud Carlos III, Spain). *Cxcr3*$^{-/-}$ mice were obtained from N. Hunt (University of Sydney, Australia), *Ccr7*$^{-/-}$ mice were obtained from W. Weninger (University of Sydney, Australia) and OT-I.*Tgfbr2f/f*.dLck-Cre mice were obtained from M. Bevan (University of Washington, USA). Bone marrow chimeras were generated by irradiation of recipient mice with 2 doses of 550 rad, 3 h apart and reconstitution with 5×10^6 donor bone marrow cells. All animal experiments were approved by The University of Melbourne Animal Ethics Committee.

Virus infections

Viruses used were the KOS strain of HSV-1 (HSV), HSV.OVA (KOS with a fusion protein of eGFP and SIINFEKL, TSYKFESV and SSIEFARL epitopes, separated by a lysine and an alanine as an attempt to ensure favorable proteasomal cleavage), WSN/NA/gB (flu.gB) and LCMV Armstrong. Epicutaneous infection by scarification was carried out using 1×10^6 PFU HSV as described[9]. For flu.gB infections, 50 PFU were administered intranasally and for LCMV infections, mice were infected with 2×10^5 PFU by i.p. injection. For HSV memory experiments, only mice with visible skin lesions during acute infection were included.

Adoptive transfer of transgenic CD8$^+$ T cells

Adoptive transfers of naïve gBT-I, OT-I or P14 cells were carried out intravenously with lymph node suspensions. Naïve gBT-I or OT-I cells were transferred at a total number of 5×10^4 cells or 2.5×10^4 cells/population in co-transfer experiments, where cell types were transferred at a ratio of 1:1. P14 cells were transferred at 5×10^5 cells. *In vitro*-generated gBT-I or OT-I effector splenocytes were activated by peptide-pulsed splenocytes as described[9]. For polyclonal activation of $CD8^+$ T cells, CD8-enriched splenocytes were activated by anti-CD3ε (145-2C11) and anti-CD28 (37.51) (5 μg/ml, eBioscience). 0.5-1 $\times 10^6$ activated cells were transferred into recipients by intradermal injection (5 × 20 μl injections over a 1 × 1.5 cm^2 area of skin) using a 30G needle. 0.5–1 $\times 10^6$ activated cells were transferred into recipients by intradermal injection. $CD8^+$ T cells were enriched using magnetic beads as described[50]. For experiments using Pertussis toxin (PTx), cells were treated *in vitro* with 100 ng/ml PTx for 90 min.

Flow cytometry and antibodies

T cells were recovered from skin as described[14]. Briefly, skin tissue was incubated for 90 min at 37 °C in dispase (2.5 mg/ml) followed by the separation of epidermis and dermis. Epidermal sheets were subsequently incubated for 30 min in trypsin/EDTA (0.25 %/0.1 %) whereas the remaining skin tissue was chopped into small fragments and incubated for 30 min at 37 °C in collagenase type 3 (3 mg/ml) and DNase (5 μg/ml). Cell suspensions were stained with antibodies for flow cytometry. The following antibodies were purchased from BD Pharmingen: APC-conjugated anti-CD45.1 (A20), PE-Cy7-conjugated anti-Va2 (B20.1), PE-conjugated anti-CD8α (53-6.7), APC eFluor780-conjugated anti-CD45.2 (104), FITC-conjugated anti-CD45.1 (A20), PE-conjugated anti-CD69 (H1.2F3), FITC-conjugated anti-CD62L (MEL-14), PE-conjugated anti-Bcl-2 (3F11), PE-conjugated anti-TNP [Bcl-2 Isotype] (A19-3), APC-Cy7-conjugated anti-TCR-beta (H57-597). The following antibodies were purchased from eBioscience: FITC-conjugated anti-CD103 (2E7), AlexaFluor700-conjugated anti-CD8α (53-6.7), Pe-Cy7-conjugated anti-CD45.1 (A20), APC-conjugated anti-CD45.2 (104), APC-conjugated anti-KLRG1 (2F1), PE-conjugated anti-CD127 (A7R34). APC-conjugated anti-CD103 (2E7) was purchased from Biolegend; APC-conjugated anti-CXCR3 (220803) and APC-conjugated Rat IgG2A Isotype control (54447) were purchased from R&D Systems. For

intracellular Bcl-2 staining, cells were fixed using a Cytofix/Cytoperm kit (BD Pharmingen) before staining with intracellular antibodies. Sphero calibration particles (BD Pharmingen) were added to samples to allow calculation of cell numbers. A FACSCanto II and Flowjo software (TreeStar) were used for analysis.

Migration assays

Ex vivo migration assays (2.5 h incubation) were done with effector gBT-I cells enriched from spleens 7 d p.i. HSV, using 24-well plates with transwell inserts (5 μm pores, Costar). The migration index was calculated as the ratio of migrated cells relative to control conditions without chemokines.

Histology

Mice were perfused with PLP buffer (P-buffer, L-lysine, 0.1 M sodium periodate with 2% paraformaldehyde) and flank skin was harvested and incubated in PLP buffer for 30 min on ice. Skin was then washed twice with PBS and incubated in 20% sucrose for 30 min at 4 °C. Tissue sections were prepared as described[5] and stained with purified rabbit anti-keratin 14 antibody (clone AF64; Covance), donkey anti-rabbit AlexaFluor647 (A31573; Invitrogen), Alexafluor conjugated-CD8 (clone 53-6.7; BD Pharmingen) or APC-conjugated KLRG1 (2F1). Images were acquired with a Zeiss LSM710 microscope and processed using Imaris 7.1 software (Bitplane).

Microarray and quantitative RT-PCR

For microarray analysis, T cells were sorted by flow cytometry from various tissues (skin: HSV 30 d p.i., gut: LCMV 60 d p.i., lung: flu.gB 30 d p.i.) using FACSAria III (BD Biosciences) and RNA extracted with Rneasy Micro Kit (Qiagen). RNA quality and quantity was determined using Bioanalyzer 2100 (Agilent) and RNA 6000 Pico Kit (Agilent). RNA was subsequently amplified and converted to cDNA using a linear amplification method; WT-Ovation Pico System (Nugen), labeled using Encore Biotin module (Nugen) and hybridized to GeneChip MouseGene 1.0 ST (Affymetrix) chips (performed at Molecular Genomics Core Facility, Peter MacCallum Cancer Centre, Australia). For qRT-PCR analysis of *Cxcl9/10* expression, RNA was extracted using

Rneasy Micro Kit (Qiagen) and cDNA synthesized with SuperScript III Reverse Transcriptase (Invitrogen) using oligo-dT primers (Promega). qRT-PCR was performed with Fast Sybergren Master mix (Life Technologies). Primer sequences were (5′-TGAAGTCCGCTGTTCTTTTCC-3′; 5′-AGTGGATCGTGCCTCGGCTG-3′) for *Cxcl9* and (5′-GTCCTAATTGCCCTTGGT-3′; 5′-TCTTGCTTCGGCAGTTAC-3′) for *Cxcl10*. For remaining qRT-PCR analysis, cell lysis and cDNA synthesis was performed using the Taqman Gene Expression cells-to-Ct kit with commercially available primers (Life Technologies). cDNA went through gene-specific amplification using Taqman Preamp master mix and inventorized Taqman assays (Life Technologies). qRT-PCR were performed with Taqman Fast Advanced Mastermix (Life Technologies) on a StepOnePlus Real-Time PCR system (Life Technologies). The threshold cycle (CT) of gene targets for each cell population were determined by RT-PCR and normalized to the CT of *Gapdh* or *Hprt* housekeeping genes (ΔCT). Relative *Cxcl9* and *Cxcl10* expression for each sample were determined using the 2^(-ΔCT) method. For other gene targets, normalized gene targets for each cell type were then compared to those of the T_{RM} population according to the 2^(-ΔΔCT) method.

Microarray analysis

All following analyses were performed in the R statistical programming environment. The raw CEL intensity files from the Affymetrix GeneChip Mouse Gene 1.0 ST arrays underwent normalization including background correction using RMA, quantile normalization, probe-specific background correction using MAS, and summarization using the median polish algorithm (doi:10.1093/nar/gng015). Minimal variability in probe intensity distributions across arrays was observed after normalization and minimal bias was seen in plots of the log intensity ratio vs. the average log intensity (MA plots). Using the log2-normalized gene expression data, principal components analysis (PCA) and pairwise entropy-based measures were used to assess the global transcriptomic differences between T cell subsets. PCA uses an orthogonal transformation to decompose the gene expression data into a set of linearly uncorrelated axes, the principal components, where PC1, PC2, etc are the axes which explain the most variation in the data, the second most, and so forth. The PC1 and PC2 axes explain 15.7% and 8.7% of variation,

respectively. PCA was visualized with XLSTAT-3Dplot (Addinsoft SARL, New York). While PCA is a useful tool for exploratory analysis of high dimensional data, the similarities/distances between T cell subsets were calculated using the mutual information (MI) across all log2-normalized gene expression probes. In this setting, MI quantifies the dependence between the transcriptomes of two T cell subsets by relating the joint distribution of gene expression probes of subsets A and B to that under the assumption that subsets A and B are independent. If subsets A and B share no information, that is they are independent, then MI = 0; if subsets A and B are identical, then their MI will be the entropy of A (or similarly, the entropy of B). Subsequent analyses used the LIMMA package to identify differentially expressed probes (DOI:10.2202/1544-6115.1027). Each T cell subset was compared against all others in a pair-wise fashion using an empirical Bayes procedure to moderate standard error and a t-test was used to test for difference in expression levels. Corresponding *P* values were corrected for multiple testing using the Benjamini-Hochberg approach. To identify the transcript signatures of T_{RM} cells, the transcriptomes of T_{RM} cells from different tissues were individually compared to those of the spleen T_{CM} cells and T_{EM} cells. Transcripts with a change in expression of 1.5 log fold change or more that satisfied the Benjamini and Hochberg adjusted *P* value of less than 0.05, from each pair-wise comparison were identified. The list of identified transcripts from all the pair-wise comparisons were then matched against one another to identify the transcript signature of individual T_{RM} populations, and the common transcript signature shared by various T_{RM} populations. Thus, a transcript must be significantly and differentially expressed in the same directionality in all resident memory when compared to all circulating memory T cell populations to be qualified as a transcript signature.

Statistical analysis

Appropriate statistical methods were chosen according to experimental setup and data distribution and are specified in the respective figure legends. Sample sizes were chosen based on previous experiences with the relevant experimental models. No specific randomization or blinding was used for the allocation to or analysis of experimental cohorts.

References

1. von Andrian, U.H. & Mackay, C.R. T-cell function and migration. Two sides of the same coin. *N. Engl. J. Med.* **343**, 1020–1034 (2000).
2. Kundig, T.M. *et al.* On the role of antigen in maintaining cytotoxic T-cell memory. *Proc. Natl. Acad. Sci. USA* **93**, 9716–9723 (1996).
3. Yang, L., Yu, Y., Kalwani, M., Tseng, T.W. & Baltimore, D. Homeostatic cytokines orchestrate the segregation of CD4 and CD8 memory T-cell reservoirs in mice. *Blood* **118**, 3039–3050 (2011).
4. Masopust, D. *et al.* Dynamic T cell migration program provides resident memory within intestinal epithelium. *J. Exp. Med.* **207**, 553–564 (2010).
5. Gebhardt, T. *et al.* Different patterns of peripheral migration by memory $CD4^+$ and $CD8^+$ T cells. *Nature* **477**, 216–219 (2011).
6. Woodland, D.L. & Kohlmeier, J.E. Migration, maintenance and recall of memory T cells in peripheral tissues. *Nat. Rev. Immunol.* **9**, 153–161 (2009).
7. Bevan, M.J. Memory T cells as an occupying force. *Eur. J. Immunol.* **41**, 1192–1195 (2011).
8. Gebhardt, T., Mueller, S.N., Heath, W.R. & Carbone, F.R. Peripheral tissue surveillance and residency by memory T cells. *Trends Immunol.* **34**, 27–32 (2013).
9. Gebhardt, T. *et al.* Memory T cells in nonlymphoid tissue that provide enhanced local immunity during infection with herpes simplex virus. *Nat. Immunol.* **10**, 524–530 (2009).
10. Kim, S.K., Reed, D.S., Heath, W.R., Carbone, F. & Lefrancois, L. Activation and migration of CD8 T cells in the intestinal mucosa. *J. Immunol.* **159**, 4295–4306 (1997).
11. Wakim, L.M., Woodward-Davis, A. & Bevan, M.J. Memory T cells persisting within the brain after local infection show functional adaptations to their tissue of residence. *Proc. Natl. Acad. Sci. USA* **107**, 17872–17879 (2010).
12. Hofmann, M. & Pircher, H. E-cadherin promotes accumulation of a unique memory CD8 T-cell population in murine salivary glands. *Proc. Natl. Acad. Sci. USA* **108**, 16741–16746 (2011).
13. Jiang, X. *et al.* Skin infection generates non-migratory memory $CD8^+$ TRM cells providing global skin immunity. *Nature* **483**, 227–231 (2012).
14. Mackay, L.K. *et al.* Long-lived epithelial immunity by tissue-resident memory T (TRM) cells in the absence of persisting local antigen presentation. *Proc. Natl. Acad. Sci. USA* **109**, 7037–7042 (2012).
15. Shin, H. & Iwasaki, A. A vaccine strategy that protects against genital herpes by establishing local memory T cells. *Nature* **491**, 463–467 (2012).
16. Sallusto, F., Lenig, D., Forster, R., Lipp, M. & Lanzavecchia, A. Two subsets of memory T lymphocytes with distinct homing potentials and effector functions. *Nature* **401**, 708–712 (1999).
17. Klonowski, K.D. *et al.* Dynamics of blood-borne CD8 memory T cell migration in vivo. *Immunity* **20**, 551–562 (2004).
18. Sheridan, B.S. & Lefrancois, L. Regional and mucosal memory T cells. *Nat. Immunol.* **12**, 485–491 (2011).

19. Kaech, S.M. & Wherry, E.J. Heterogeneity and cell-fate decisions in effector and memory CD8$^+$ T cell differentiation during viral infection. *Immunity* **27**, 393–405 (2007).
20. Obar, J.J. & Lefrancois, L. Early events governing memory CD8$^+$ T-cell differentiation. *Int. Immunol.* **22**, 619–625 (2010).
21. Masopust, D., Vezys, V., Marzo, A.L. & Lefrancois, L. Preferential localization of effector memory cells in nonlymphoid tissue. *Science* **291**, 2413–2417 (2001).
22. Masopust, D., Vezys, V., Wherry, E.J., Barber, D.L. & Ahmed, R. Cutting edge: gut microenvironment promotes differentiation of a unique memory CD8$^+$ T cell population. *J. Immunol.* **176**, 2079–2083 (2006).
23. Tang, V.A. & Rosenthal, K.L. Intravaginal infection with herpes simplex virus type-2 (HSV-2) generates a functional effector memory T cell population that persists in the murine genital tract. *J. Reprod. Immunol.* **87**, 39–44 (2010).
24. Kane, C.J., Knapp, A.M., Mansbridge, J.N. & Hanawalt, P.C. Transforming growth factor-beta 1 localization in normal and psoriatic epidermal keratinocytes in situ. *J. Cell Physiol.* **144**, 144–150 (1990).
25. Koyama, S.Y. & Podolsky, D.K. Differential expression of transforming growth factors alpha and beta in rat intestinal epithelial cells. *J. Clin. Invest.* **83**, 1768–1773 (1989).
26. Wang, D. *et al.* Regulation of CD103 expression by CD8$^+$ T cells responding to renal allografts. *J. Immunol.* **172**, 214–221 (2004).
27. Lee, Y.T. *et al.* Environmental and antigen receptor-derived signals support sustained surveillance of the lungs by pathogen-specific cytotoxic T lymphocytes. *J. Virol.* **85**, 4085–4094 (2011).
28. Casey, K.A. *et al.* Antigen-independent differentiation and maintenance of effector-like resident memory T cells in tissues. *J. Immunol.* **188**, 4866–4875 (2012).
29. Spangrude, G.J., Sacchi, F., Hill, H.R., Van Epps, D.E. & Daynes, R.A. Inhibition of lymphocyte and neutrophil chemotaxis by pertussis toxin. *J. Immunol.* **135**, 4135–4143 (1985).
30. Bromley, S.K., Thomas, S.Y. & Luster, A.D. Chemokine receptor CCR7 guides T cell exit from peripheral tissues and entry into afferent lymphatics. *Nat. Immunol.* **6**, 895–901 (2005).
31. Debes, G.F. *et al.* CC chemokine receptor 7 expression by effector/memory CD4+ T cells depends on antigen specificity and tissue localization during influenza A virus infection. *J. Virol.* **78**, 7528–7535 (2004).
32. Kaech, S.M., Hemby, S., Kersh, E. & Ahmed, R. Molecular and functional profiling of memory CD8 T cell differentiation. *Cell* **111**, 837–851 (2002).
33. El-Asady, R. *et al.* TGF-{beta}-dependent CD103 expression by CD8$^+$ T cells promotes selective destruction of the host intestinal epithelium during graft-versus-host disease. *J. Exp. Med.* **201**, 1647–1657 (2005).
34. Tripp, R.A., Hou, S. & Doherty, P.C. Temporal loss of the activated L-selectin-low phenotype for virus-specific CD8$^+$ memory T cells. *J. Immunol.* **154**, 5870–5875 (1995).
35. Wherry, E.J. *et al.* Lineage relationship and protective immunity of memory CD8 T cell subsets. *Nat. Immunol.* **4**, 225–234 (2003).

36. Kaech, S.M. *et al*. Selective expression of the interleukin 7 receptor identifies effector CD8 T cells that give rise to long-lived memory cells. *Nat. Immunol.* **4**, 1191–1198 (2003).
37. Sarkar, S. *et al*. Functional and genomic profiling of effector CD8 T cell subsets with distinct memory fates. *J. Exp. Med.* **205**, 625–640 (2008).
38. Wakim, L.M., Waithman, J., van Rooijen, N., Heath, W.R. & Carbone, F.R. Dendritic cell-induced memory T cell activation in nonlymphoid tissues. *Science* **319**, 198–202 (2008).
39. Cuburu, N. *et al*. Intravaginal immunization with HPV vectors induces tissue-resident $CD8^+$ T cell responses. *J. Clin. Invest.* **122**, 4606–4620 (2012).
40. Debes, G.F. *et al*. Chemokine receptor CCR7 required for T lymphocyte exit from peripheral tissues. *Nat. Immunol.* **6**, 889–894 (2005).
41. Wakim, L.M. *et al*. The molecular signature of tissue resident memory $CD8^+$ T cells isolated from the brain. *J. Immunol.* **189**, 3462–3471 (2012).
42. Matloubian, M. *et al*. Lymphocyte egress from thymus and peripheral lymphoid organs is dependent on S1P receptor 1. *Nature* **427**, 355–360 (2004).
43. Skon, C.N. *et al*. Transcriptional downregulation of S1PR1 is required for establishment of resident memory $CD8^+$ T cells. *Nat. Immunol.* **In press** (2013).
44. Shiow, L.R. *et al*. CD69 acts downstream of interferon-alpha/beta to inhibit S1P1 and lymphocyte egress from lymphoid organs. *Nature* **440**, 540–544 (2006).
45. Jenne, C.N. *et al*. T-bet-dependent S1P5 expression in NK cells promotes egress from lymph nodes and bone marrow. *J. Exp. Med.* **206**, 2469–2481 (2009).
46. Druey, K.M., Blumer, K.J., Kang, V.H. & Kehrl, J.H. Inhibition of G-protein-mediated MAP kinase activation by a new mammalian gene family. *Nature* **379**, 742–746 (1996).
47. Gebhardt, T. & Mackay, L.K. Local immunity by tissue-resident $CD8^+$ memory T cells. *Front. Immunol.* **3**, 340 (2012).
48. Jameson, J. *et al*. A role for skin gammadelta T cells in wound repair. *Science* **296**, 747–749 (2002).
49. Sharp, L.L., Jameson, J.M., Cauvi, G. & Havran, W.L. Dendritic epidermal T cells regulate skin homeostasis through local production of insulin-like growth factor 1. *Nat. Immunol.* **6**, 73–79 (2005).
50. Waithman, J., Gebhardt, T., Davey, G.M., Heath, W.R. & Carbone, F.R. Cutting edge: Enhanced IL-2 signaling can convert self-specific T cell response from tolerance to autoimmunity. *J. Immunol.* **180**, 5789–5793 (2008).

Table 1: Differentially expressed transcripts shared by Trms relative to Tcm, and to Tem

Gene symbol	Gene name	Entrez ID	Probe ID	Differential expression relative to Tcm, and to Tem
Cd244	CD244 natural killer cell receptor 2B4	18106	10351644	Up
Cdh1	cadherin 1	12550	10575052	Up
Chn2	chimerin (chimaerin) 2	69993	10538356	Up
Ctla4	cytotoxic T-lymphocyte-associated protein 4	12477	10346790	Up
Hpgds	hematopoietic prostaglandin D synthase	54486	10545101	Up
Hspa1a	heat shock protein 1A	193740	10450369	Up
Hspa1a	heat shock protein 1A	193740	10444589	Up
Hspa1a	heat shock protein 1A	193740	10450367	Up
Icos	inducible T-cell co-stimulator	54167	10346799	Up
Inpp4b	inositol polyphosphate-4-phosphatase, type II	234515	10573082	Up
Itga1	integrin alpha 1	109700	10412298	Up
Itgae	integrin alpha E, epithelial-associated	16407	10378286	Up
Litaf	LPS-induced TN factor	56722	10437687	Up
LOC100503878	zinc finger protein 683-like	100503878	10508909	Up
LOC641050	hypothetical protein LOC641050	641050	10504761	Up
LOC641050	hypothetical protein LOC641050	641050	10538892	Up
Nr4a1	nuclear receptor subfamily 4, group A, member 1	15370	10427035	Up
Nr4a2	nuclear receptor subfamily 4, group A, member 2	18227	10482772	Up
Qpct	glutaminyl-peptide cyclotransferase (glutaminyl cyclase)	70536	10447056	Up
Rgs1	regulator of G-protein signaling 1	50778	10358408	Up
Rgs2	regulator of G-protein signaling 2	19735	10358389	Up
Sik1	salt inducible kinase 1	17691	10449741	Up
Skil	SKI-like	20482	10491300	Up
Tmem123	transmembrane protein 123	71929	10583145	Up
Vps37b	vacuolar protein sorting 37B (yeast)	330192	10533729	Up
Xcl1	chemokine (C motif) ligand 1	16963	10359697	Up
Cmah	cytidine monophospho-N-acetylneuraminic acid hydroxylase	12763	10404132	Down
Elovl7	ELOVL family member 7, elongation of long chain fatty acids (yeast)	74559	10407072	Down
Eomes	eomesodermin homolog (Xenopus laevis)	13813	10589994	Down
Fam65b	family with sequence similarity 65, member B	193385	10404152	Down
Fgf13	fibroblast growth factor 13	14168	10604751	Down
Klre1	killer cell lectin-like receptor family E member 1	243655	10542205	Down
Ly6c2	lymphocyte antigen 6 complex, locus C2	100041546	10429573	Down
Rasgrp2	RAS, guanyl releasing protein 2	19395	10460968	Down
S1pr1	sphingosine-1-phosphate receptor 1	13609	10501586	Down
S1pr5	sphingosine-1-phosphate receptor 5	94226	10591494	Down
Sidt1	SID1 transmembrane family, member 1	320007	10439583	Down
Slamf6	SLAM family member 6	30925	10351691	Down
Tlr1	toll-like receptor 1	21897	10530145	Down
Usp33	ubiquitin specific peptidase 33	170822	10496919	Down

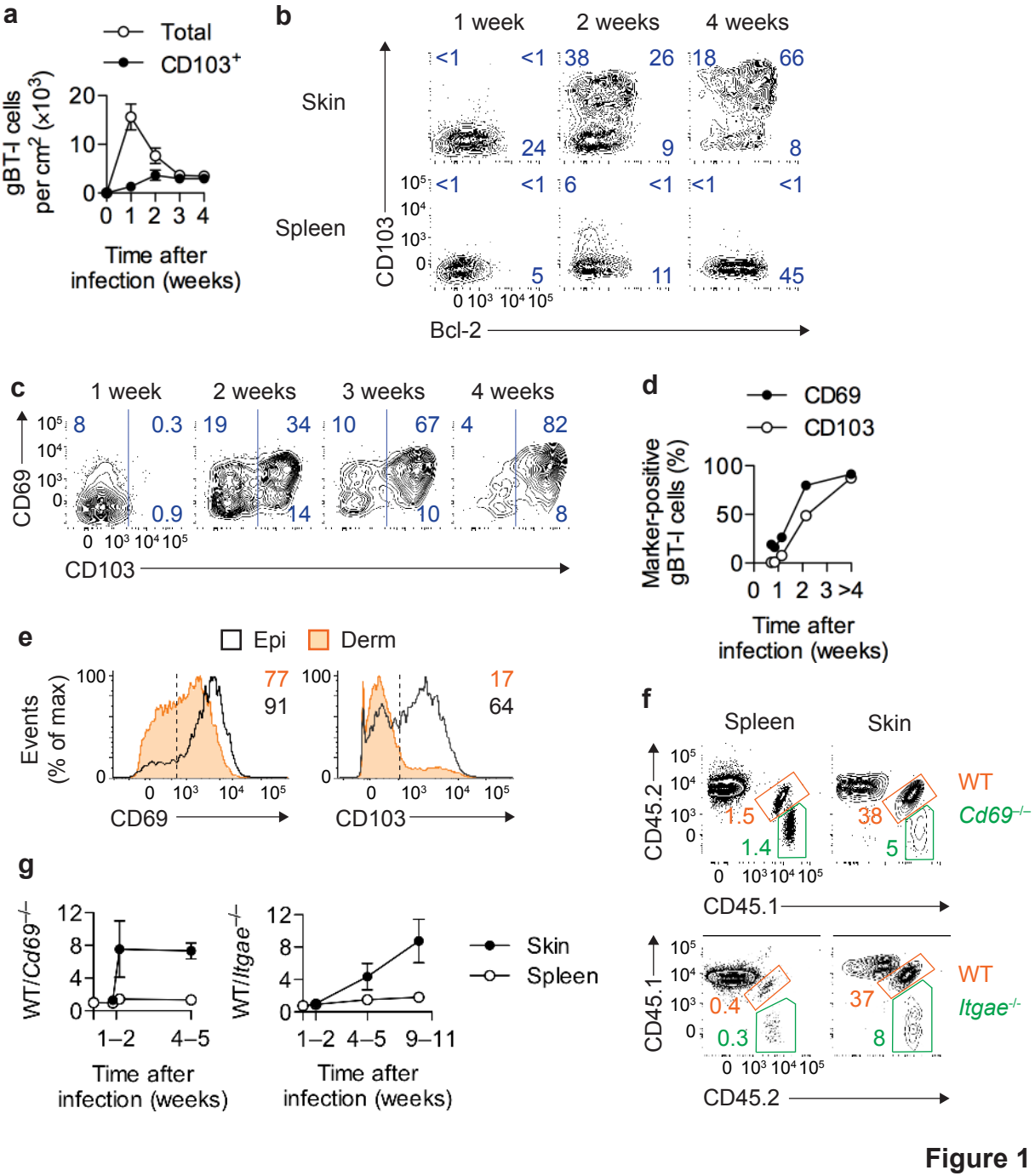
a
Total
CD103+
gBT-I cells per cm2 (×10^3)
20
10
0
0 1 2 3 4
Time after infection (weeks)
b
1 week
2 weeks
4 weeks
Skin
Spleen
CD103
<1
<1
38
26
18
66
24
9
8
<1
<1
6
<1
<1
<1
5
11
45
0 10^3 10^4 10^5
Bcl-2
c
1 week
2 weeks
3 weeks
4 weeks
CD69
8
0.3
19
34
10
67
4
82
0.9
14
10
8
CD103
d
CD69
CD103
Marker-positive gBT-I cells (%)
100
50
0
0 1 2 3 >4
Time after infection (weeks)
e
Epi
Derm
Events (% of max)
100
77
91
17
64
CD69
CD103
f
Spleen
Skin
CD45.2
1.5
1.4
38
5
WT
Cd69−/−
CD45.1
0.4
0.3
37
8
WT
Itgae−/−
g
WT/Cd69−/−
WT/Itgae−/−
12
8
4
0
1–2
4–5
9–11
Time after infection (weeks)
Skin
Spleen

Figure 1

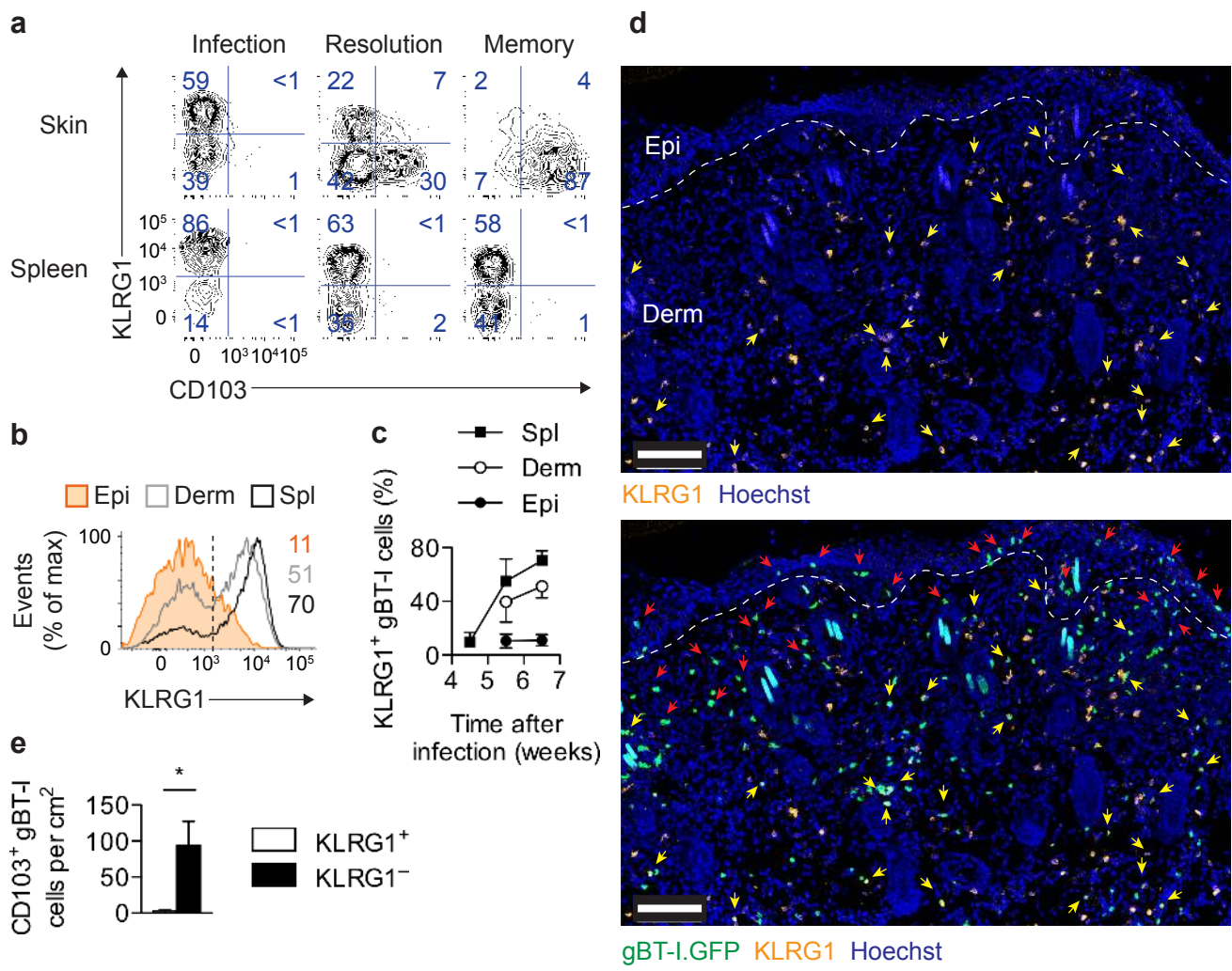
a
Infection
Resolution
Memory
Skin
Spleen
KLRG1
CD103
59
<1
39
1
22
7
42
30
2
4
7
87
86
<1
14
<1
63
<1
35
2
58
<1
47
1
0
10³
10⁴
10⁵
b
Epi
Derm
Spl
Events (% of max)
100
0
11
51
70
KLRG1
c
Spl
Derm
Epi
KLRG1⁺ gBT-I cells (%)
80
40
0
4
5
6
7
Time after infection (weeks)
d
Epi
Derm
KLRG1 Hoechst
gBT-I.GFP KLRG1 Hoechst
e
CD103⁺ gBT-I cells per cm²
150
100
50
0
*
KLRG1⁺
KLRG1⁻

Figure 2

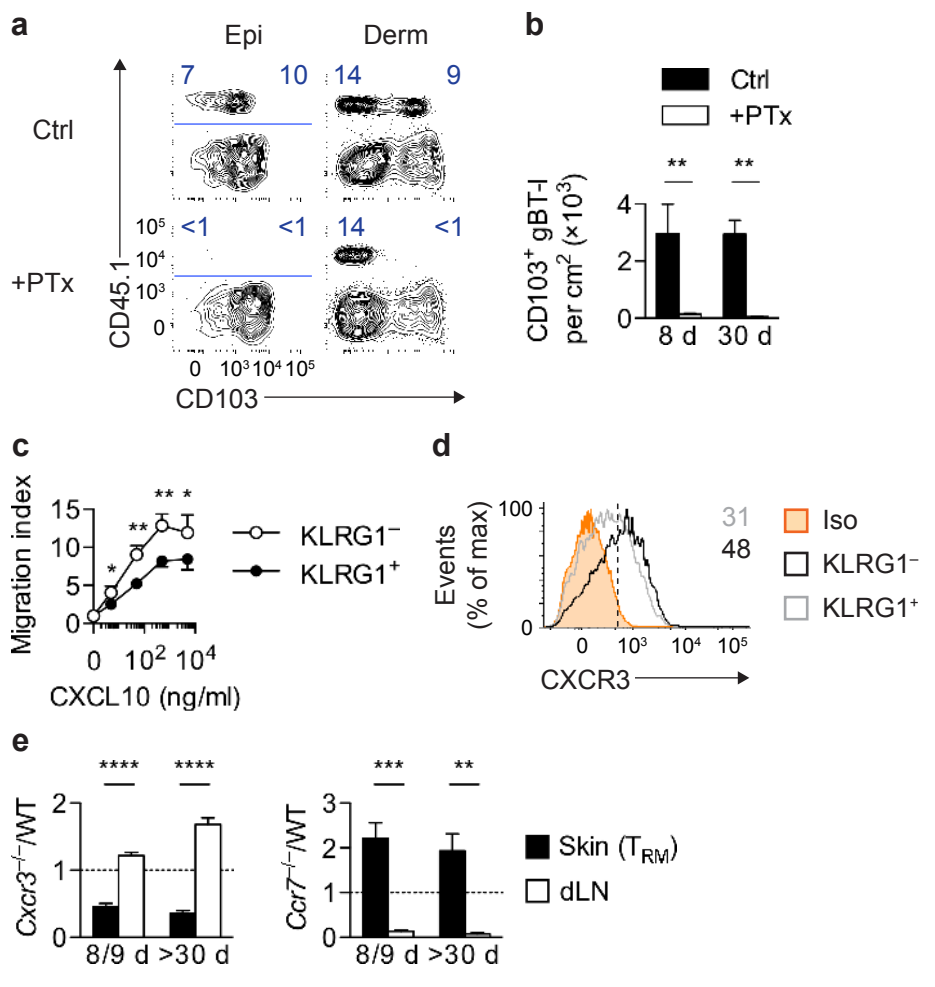
a
Epi
Derm
Ctrl
+PTx
7
10
14
9
<1
<1
14
<1
CD45.1
CD103
b
Ctrl
+PTx
**
**
CD103+ gBT-I per cm2 (×10^3)
8 d
30 d
c
Migration index
KLRG1−
KLRG1+
CXCL10 (ng/ml)
d
Events (% of max)
31
48
Iso
KLRG1−
KLRG1+
CXCR3
e
****
****
***
**
Cxcr3−/−/WT
Ccr7−/−/WT
8/9 d
>30 d
Skin (TRM)
dLN

Figure 3

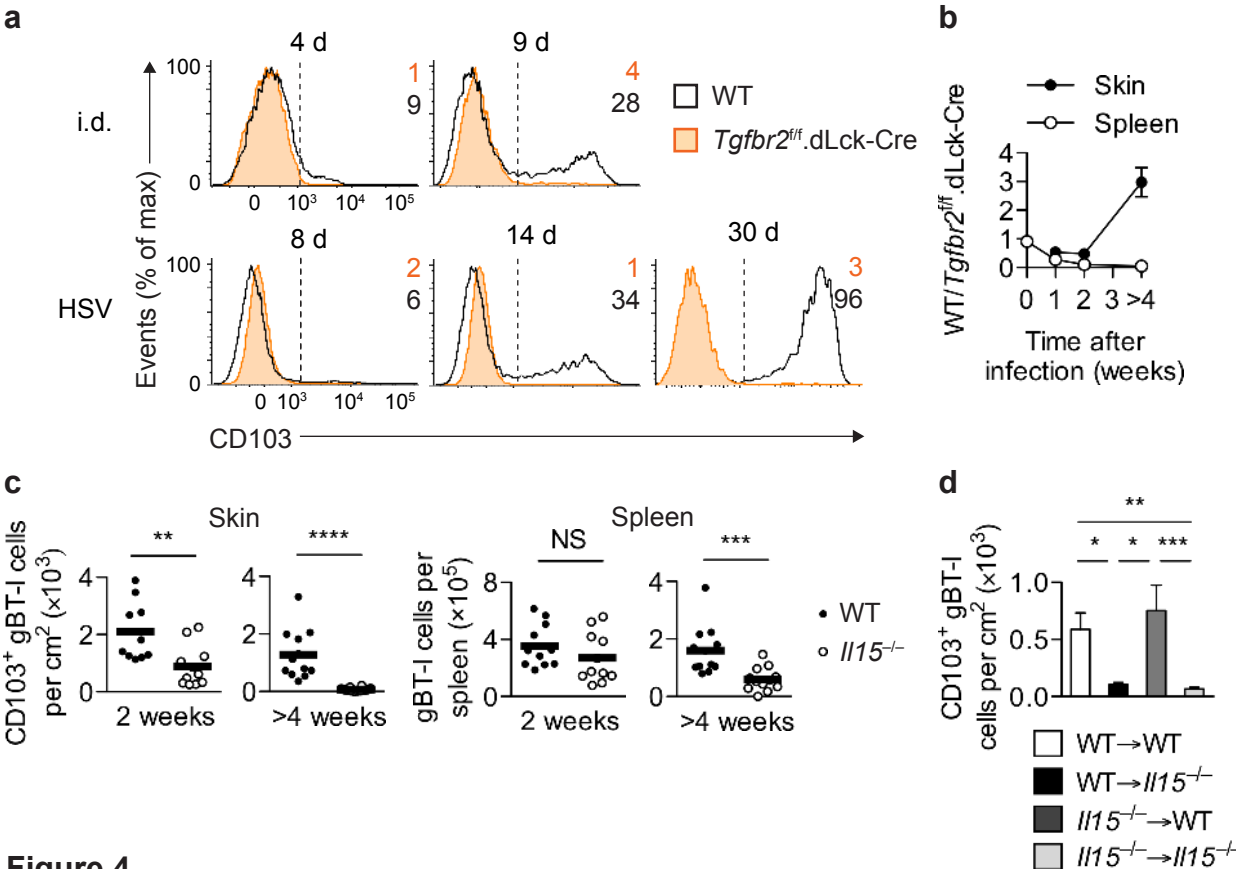
a
4 d
9 d
8 d
14 d
30 d
i.d.
HSV
Events (% of max)
CD103
1
9
4
28
2
6
1
34
3
96
WT
Tgfbr2f/f.dLck-Cre
b
Skin
Spleen
WT/Tgfbr2f/f.dLck-Cre
Time after infection (weeks)
c
Skin
Spleen
CD103+ gBT-I cells per cm2 (×10^3)
gBT-I cells per spleen (×10^5)
2 weeks
>4 weeks
NS
WT
Il15−/−
d
CD103+ gBT-I cells per cm2 (×10^3)
WT→WT
WT→Il15−/−
Il15−/−→WT
Il15−/−→Il15−/−

Figure 4

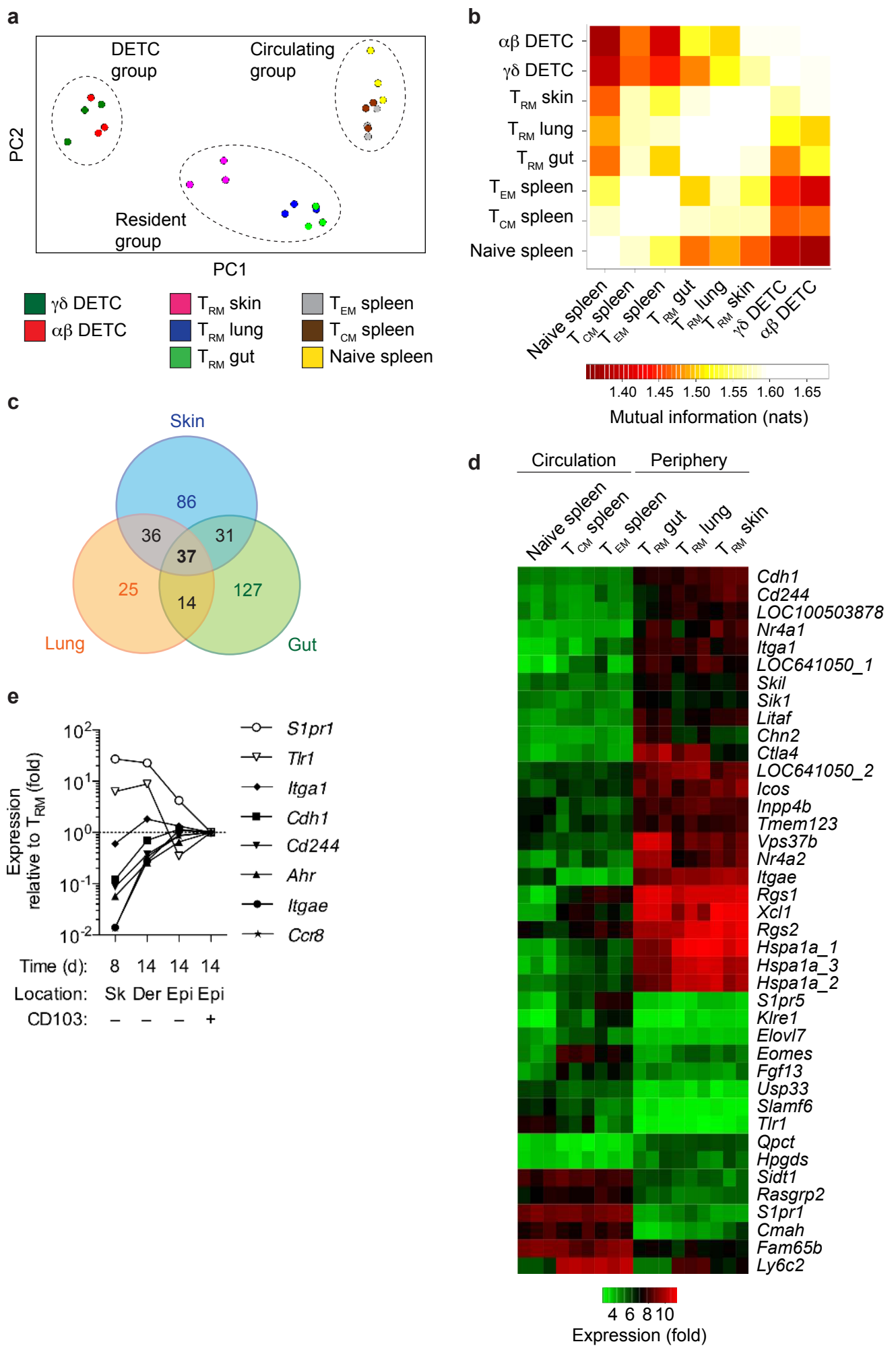
a
DETC group
Circulating group
Resident group
PC2
PC1
γδ DETC
αβ DETC
T_RM skin
T_RM lung
T_RM gut
T_EM spleen
T_CM spleen
Naive spleen
b
αβ DETC
γδ DETC
T_RM skin
T_RM lung
T_RM gut
T_EM spleen
T_CM spleen
Naive spleen
1.40 1.45 1.50 1.55 1.60 1.65
Mutual information (nats)
c
Skin
Lung
Gut
86
36
31
37
25
127
14
d
Circulation
Periphery
Cdh1
Cd244
LOC100503878
Nr4a1
Itga1
LOC641050_1
Skil
Sik1
Litaf
Chn2
Ctla4
LOC641050_2
Icos
Inpp4b
Tmem123
Vps37b
Nr4a2
Itgae
Rgs1
Xcl1
Rgs2
Hspa1a_1
Hspa1a_3
Hspa1a_2
S1pr5
Klre1
Elovl7
Eomes
Fgf13
Usp33
Slamf6
Tlr1
Qpct
Hpgds
Sidt1
Rasgrp2
S1pr1
Cmah
Fam65b
Ly6c2
4 6 8 10
Expression (fold)
e
Expression relative to T_RM (fold)
S1pr1
Tlr1
Itga1
Cdh1
Cd244
Ahr
Itgae
Ccr8
Time (d): 8 14 14 14
Location: Sk Der Epi Epi
CD103: – – – +

Figure 5

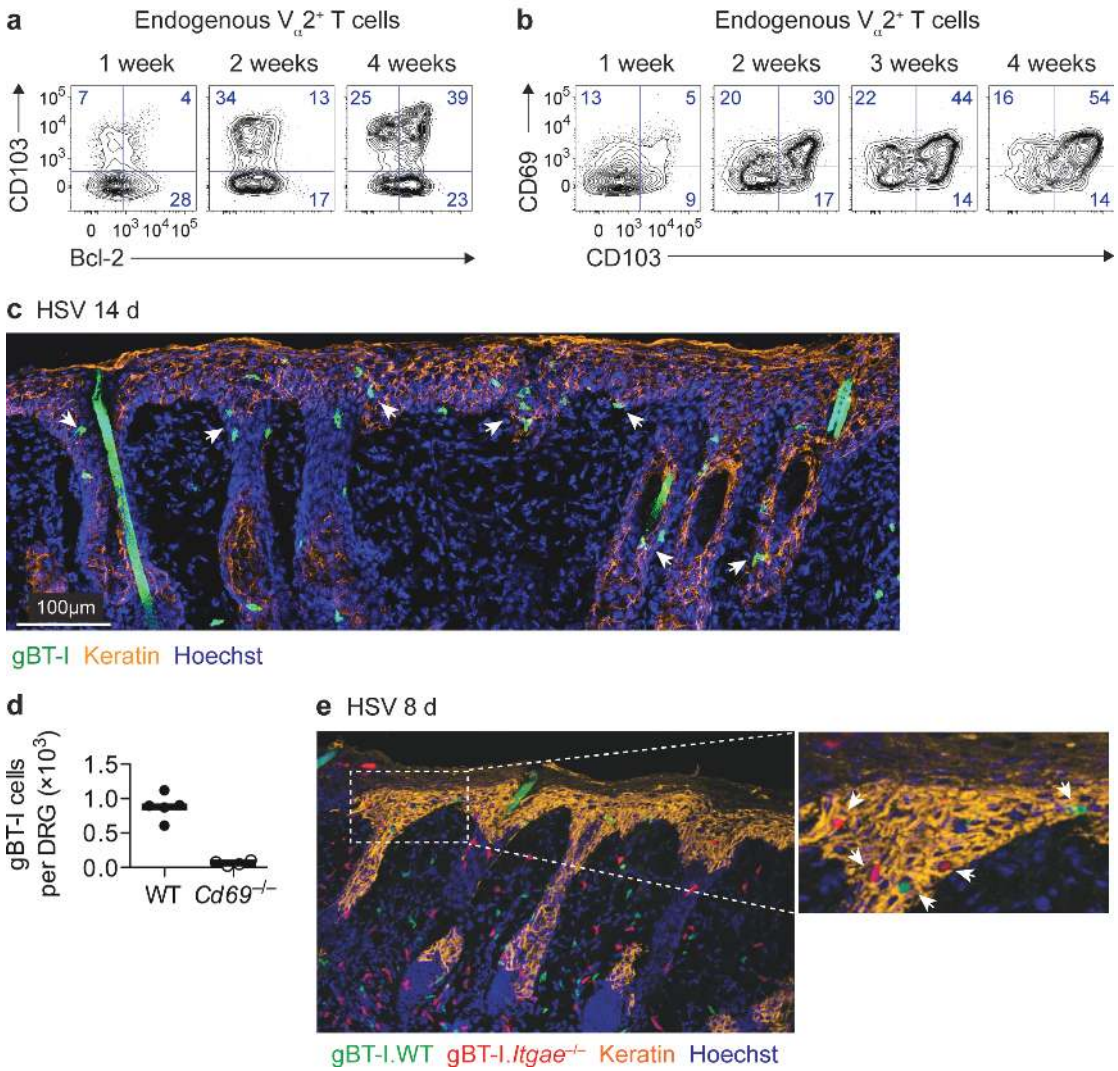

Supplementary Figure 1. Phenotype and anatomical localization of T_{RM} cells. (**a**,**b**) Analysis of CD103, Bcl-2 and CD69 expression by endogenous $V_\alpha2^+$ T cells in skin at the indicated times p.i. Plots are gated on $V_\alpha2^+$ CD45.2$^+$ cells; numbers indicate the percentage of events in the respective gates. Data representative of 2–3 experiments. (**c**) Mice received naïve gBT-I.GFP cells prior to HSV infection. Arrows indicate examples of gBT-I.GFP cells in the epidermis and hair follicle epithelium 14 d p.i. Photo representative of >5 experiments. (**d**) Wild-type (WT) and *Cd69*$^{-/-}$ gBT-I cells were transferred into WT mice prior to HSV infection. Enumeration of gBT-I cells in dorsal root ganglia (DRG) 30 d p.i. Data from one experiment (*n* = 5 mice/group). (**e**) WT (GFP-expressing, green) and *Itgae*$^{-/-}$ (DsRed-expressing, red) gBT-I cells were co-transferred into WT mice prior to HSV infection. Microscopy of skin 8 d p.i. Staining with anti-keratin antibody to delineate the epidermis and hair follicle epithelium. Arrows in insert indicate gBT-I cells in the epidermis. Photo representative of *n* = 3 mice analyzed.

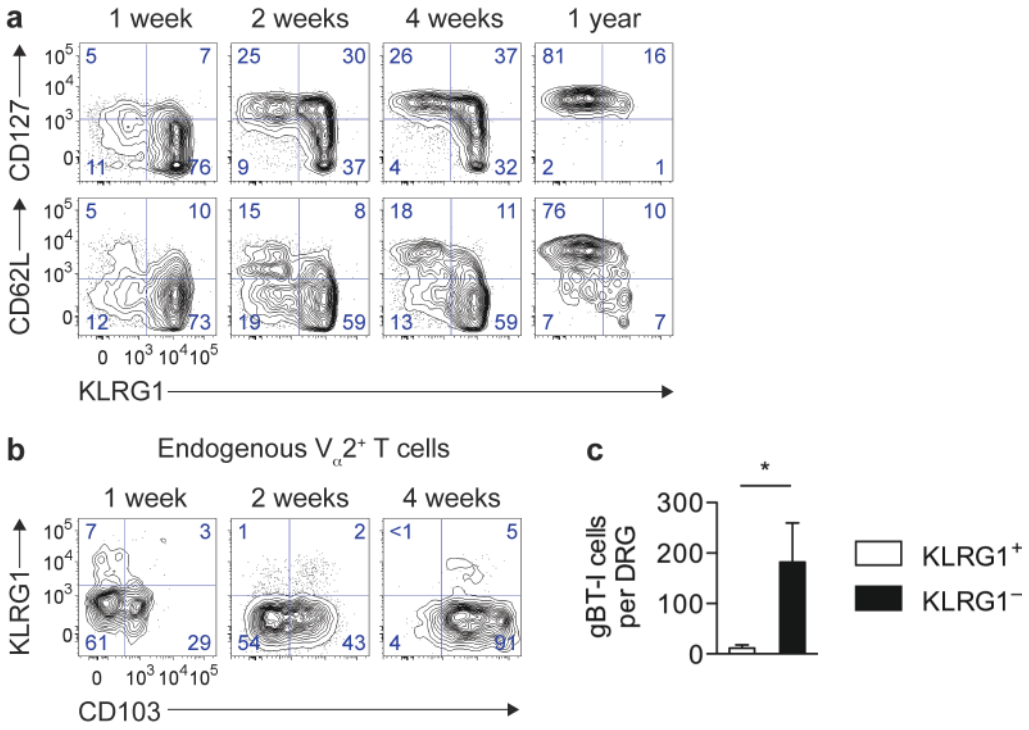

Supplementary Figure 2. Development of virus-specific CD8$^+$ memory T cells after HSV-1 skin infection. (**a**) Mice received naïve gBT-I cells prior to infection. Analysis of CD62L, CD127 and KLRG1 expression by gBT-I cells in the spleen at different time points after infection. Plots are gated on V$_\alpha$2$^+$CD45.2$^+$CD45.1$^+$ cells and are representative of *n* = 4–8 mice/time point. Numbers indicate the percentage of events in the respective gates (as in **b**). (**b**) Analysis of CD103 and KLRG1 expression by endogenous V$_\alpha$2$^+$ T cells in skin at the indicated times p.i. Plots are gated on V$_\alpha$2$^+$CD45.2$^+$ cells and are representative of 3 experiments (*n* = 12 mice/time point). (**c**) Effector gBT-I cells were sorted into KLRG1$^+$ and KLRG1$^-$ subsets from spleens of infected mice (6 d p.i.) and transferred into infected recipients (4 d p.i.). Enumeration of CD103$^+$ gBT-I cells in dorsal root ganglia (DRG) 3 weeks p.i. Data from 3 experiments (*n* = 12 mice/group); *, *P* < 0.05 by two-tailed Mann-Whitney test.

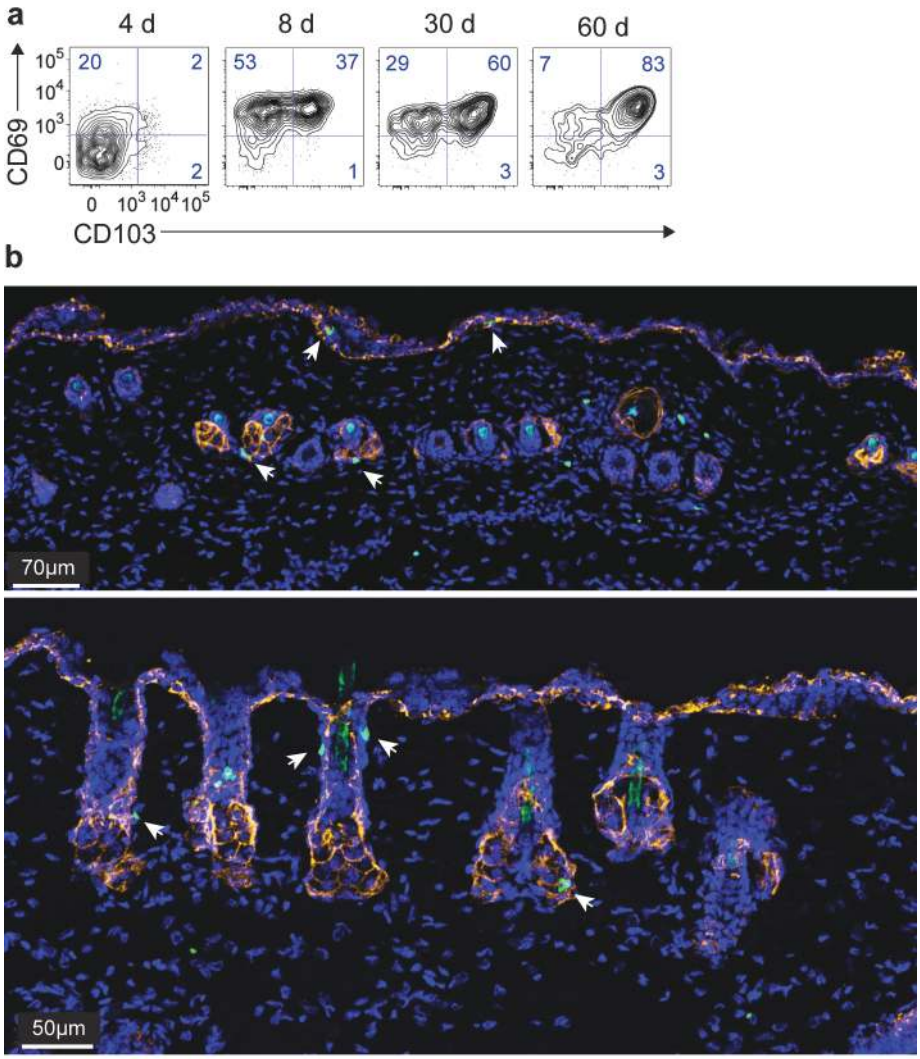
a
4 d
8 d
30 d
60 d
CD69
CD103
20
2
2
53
37
1
29
60
3
7
83
3
b
70µm
50µm
gBT-I.GFP Keratin Hoechst
c
100µm
gBT-I (Ctrl) gBT-I (+PTx) Keratin Hoechst
d
Ctrl
+PTx
Events (% of max)
+TGF-β
+TGF-β
CD103

Supplementary Figure 3. Epidermal localization of CD8$^+$ T cells after intradermal transfer. (**a**) CD103 and CD69 expression by gBT-I cells in skin at the indicated times after *in vitro* activation by gB peptide-coated splenocytes and intradermal transfer. Plots are gated on Vα2$^+$CD45.2$^+$CD45.1$^+$ cells and are representative of 2–3 experiments (*n* = 6–12 mice/time point). Numbers indicate the percentage of events in the respective gates. (**b**) *In vitro* activated gBT-I.GFP cells were transferred into the skin by intradermal injection. Microscopy of skin 30 d after transfer. Staining with anti-keratin antibody to denote epithelium in the epidermis and hair follicles. Arrows indicate examples of gBT-I.GFP cells (green). Photos (2 examples shown) are representative of 2 experiments. (**c**) *In vitro* activated gBT-I cells were left untreated (Ctrl, DsRed-expressing, red) or treated with PTx (+PTx, GFP-expressing, green) and co-transferred into mice by intradermal injection. Microscopy of skin 4 weeks after transfer; anti-keratin staining denotes the epidermal layer and hair follicle epithelium. Red arrows indicate control cells in the epithelium, green arrows indicate PTx-treated cells in the dermis. Photos representative of 2 experiments. (**d**) *In vitro* activated gBT-I cells were untreated (Ctrl) or treated with PTx (+PTx). Analysis of CD103 expression following subsequent *in vitro* incubation of the cells in the presence (solid or dashed black lines, as indicated) or absence (orange area) of TGF-β (5 ng/ml; 24 hours). Plots are gated on Vα2$^+$CD45.2$^+$CD45.1$^+$ cells and are representative of 2 experiments.

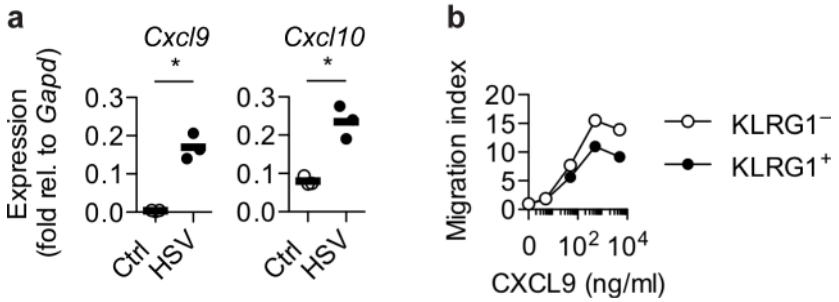

Supplementary Figure 4. Chemokine expression in skin and *ex vivo* migration of KLRG1$^+$ and KLRG1$^-$ effector cells. (**a**) mRNA expression for genes encoding CXCL9 and CXCL10 in CD45.2$^-$EpCAM$^+$ keratinocytes sorted from naïve (Ctrl) or HSV-infected skin (d 6 p.i.). Data pooled from 3 independent experiments (represented by individual symbols). *, $P < 0.05$ by two-tailed paired *t*-test. (**b**) *Ex vivo* migration towards CXCL9 gradients by KLRG1$^+$ (closed symbols) and KLRG1$^-$ (open symbols) gBT-I cells enriched from spleens 7 d after HSV skin infection (cells pooled from $n = 5$ donor mice).

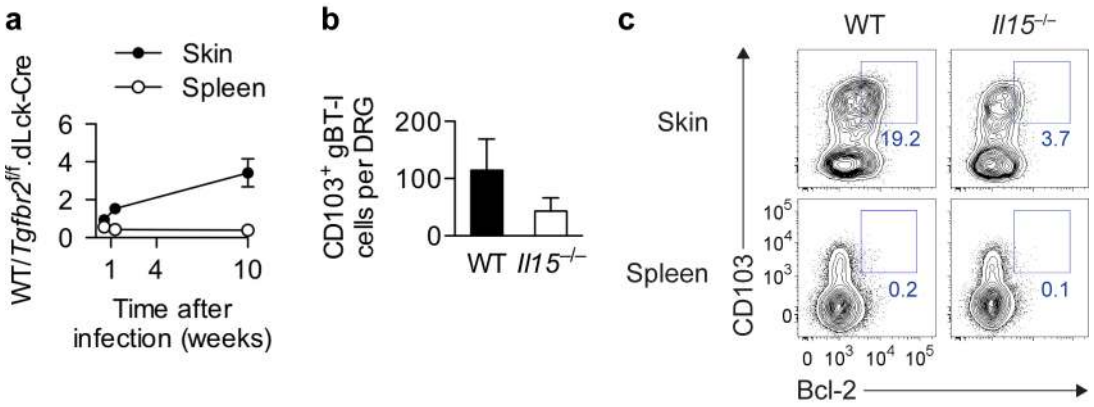

Supplementary Figure 5. Requirement of TGF-β receptor and IL-15 signaling in the development of CD103$^+$ T_{RM} cells. (**a**) Wild-type (WT) and TGF-R-deficient (*Tgfbr2f/f*.dLck-Cre) OT-I cells were activated by culture with ovalbumin peptide-coated splenocytes and transferred into the skin by intradermal injection. Depicted are the ratios of WT relative to *Tgfbr2f/f*.dLck-Cre cells in the skin and spleen at the indicated times after transfer. Data representative of 2 experiments (*n* = 3–4 mice/group). (**b**,**c**) Effector gBT-I cells were enriched from spleens of WT mice (6 d p.i.) and transferred into infected (4 d p.i.) WT or *Il15*$^{-/-}$ recipient mice. (**b**) Enumeration of CD103$^+$ gBT-I cells in dorsal root ganglia (DRG) 4 wks p.i. Data from one experiment with *n* = 5 mice/group. (**c**) CD103 and Bcl-2 expression by gBT-I cells in WT and *Il15*$^{-/-}$ mice (11 d p.i.). Plots are gated on V_a2^+CD45.2$^+$CD45.1$^+$ cells; numbers depict percentages of events in the respective gates. Data are representative of 2 experiments (*n* = 8 mice/group).

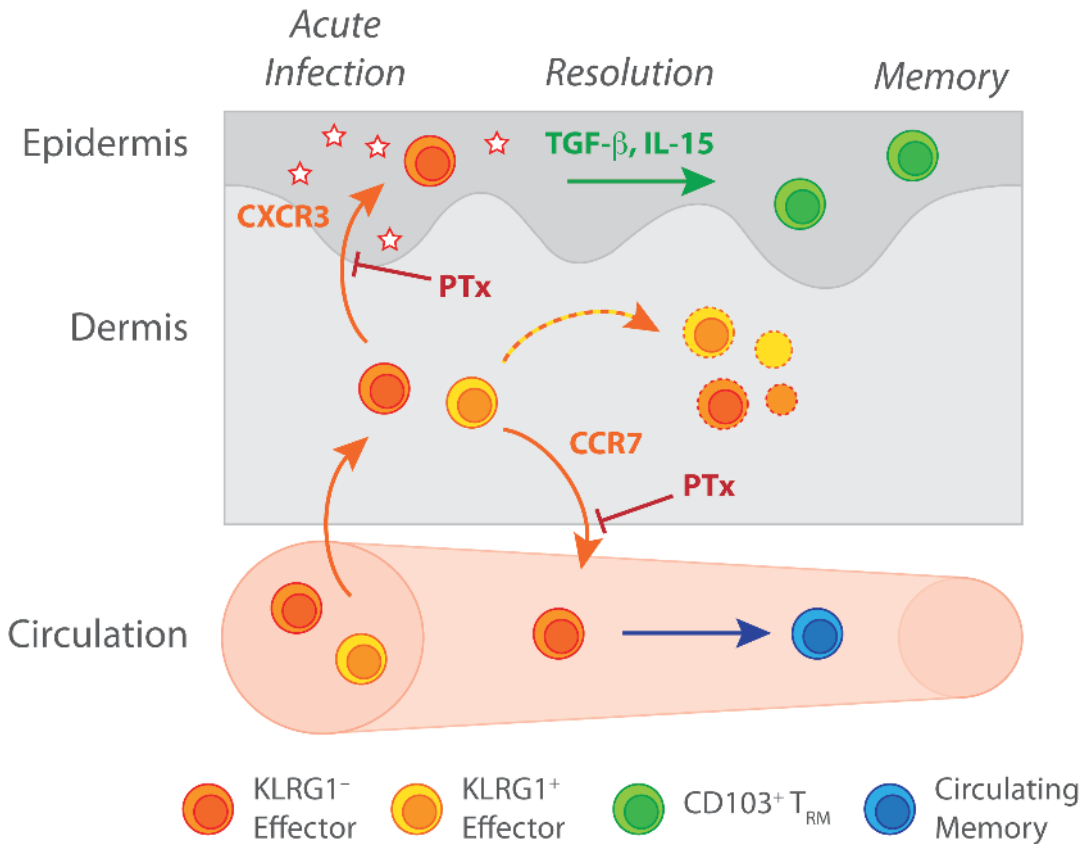

Supplementary Figure 6. The developmental pathway for the formation of T_{RM} cells. KLRG1$^-$ T_{RM} precursors enter the dermis where they may (i) die *in situ*, (ii) exit the skin and return to the blood in a CCR7-dependent manner or (iii) migrate to the epidermis, partly under the influence of CXCR3 ligands. Both tissue exit and epidermal entry are sensitive to treatment with pertussis toxin (PTx) indicating the involvement of G protein-coupled molecules such as chemokine receptors. Following epidermal entry, T_{RM} precursors undergo maturation into long-lived CD103$^+$ T_{RM} cells in a TGF-β- and IL-15-dependent manner. Epithelial T_{RM} cells and their counterparts in the circulation are depicted with different symbols to highlight their distinct transcriptional profiles.